Mon. Not. R. Astron. Soc. **000**, 1–9 (2012) Printed 11 February 2013 (MN LATEX style file v2.2)

What can we gain from magnification bias as a complement to shear?

Christopher Duncan[1], Alan Heavens[2], Catherine Heymans[1], Benjamin Joachimi[1]
[1] *Institute for Astronomy, Royal Observatory Edinburgh, Blackford Hill, Edinburgh*
[2] *Imperial College London*

Submitted

ABSTRACT
With the wealth of upcoming data from wide-field surveys such as KiDS, Pan-STARRS, DES and Euclid, it is more important than ever to understand the full range of independent probes of cosmology at our disposal. With this in mind, we motivate the use of cosmic magnification as a probe of cosmology, presenting forecasts for the improvements to cosmic shear cosmological parameter constraints when cosmic magnification is included for a KiDS-like survey. We find that when uncertainty in the galaxy bias is factored into the forecasts, cosmic magnification is less powerful that previously reported, but as it is less likely to be prone to measurement error we conclude it is a useful tool for cosmological analyses.

Key words: gravitational lensing: weak, magnification, shear – cosmology

1 INTRODUCTION

As light from distant galaxies propagates through the Universe, it's path can be deflected by the local matter distribution, an effect called gravitational lensing. As a result, when we view distant galaxies we observe both a change in the shape of it's image, as well as a change in it's position and size. Cosmic shear is the study of the first of these effects, and statistical analysis using galaxy ellipticities has proven a very promising tool for probing cosmology (see Bartlemann and Schneider for a review). However, as shear analysis requires accurate shape measurement, it's measurement has proven a particularly difficult task [ref Great], with measurements sensitive to the Point Spread Function and pixelisation, as well as physical contamination from intrinsic galaxy alignments.

With many current and upcoming large scale surveys such as CFHT, DES and Euclid, it is becoming more important than ever to understand what gains there are to be made in exploiting the other half of the lensing signal. As well as a distortion in the observed shape of a galaxy, gravitational lensing by foreground large scale structure can cause the amplification of the flux of sources as their size is magnified, and a change in their observed positions. Direct observations of the induced change in size of a lensed body is the most obvious measure of the magnification effect, and magnification has been successfully detected using a combination of the change in sizes of a lensed population of galaxies and a change in their magnitudes in [ref Schmidt]. However, due to the nature of the measurements required to detect size change due to magnification, it suffers from many of the same systematics listed for cosmic shear above. In [ref Buise] it was shown that these systematics may limit the use of size change for ground based surveys where the effects of PSF are largest, however for space based surveys with smaller PSF and higher signal to noise, the statistical power of size magnification can rival cosmic shear, and may be an excellent complement to shear analyses.

Another recent technique to use the magnification part of the lensing signal uses a fundamental plane relation to relate the effective radius of galaxy, which is altered by magnification, to the galaxies surface brightness and stellar velocity dispersion, both of which remain unaltered.

The most common technique uses fluctuations in the observed number density of sources as a probe of magnification, called magnification bias. Observationally, the observed number density of sources is altered due to magnification in two ways, the dilution of sources as the solid angle behind the lens is stretched, and the (de-)amplification of sources as their fluxes are (de-)magnified below or above the survey flux limit. Lensing can therefore induce non-vanishing angular number density contrast correlations between a background distribution of sources and foreground large scale structure which are sensitive to cosmology through the distribution of matter and it's evolution, and distance measures.

The early history of using magnification bias to measure magnification proved controversial with early attempts at measuring changes in number density of a background set of quasars due to foreground LSS commonly in disagreement, and with measurements that gave amplitudes of correlations far larger than theoretical predictions (ref Scranton et al provides a concise summary of early literature). However, the successful measurement of number density contrast correla-

tions between background quasars and foreground galaxies using the Sloan Digital Sky Survey in (ref Scranton 2005), and later using high redshift Lyman break galaxies as the background in CARS (ref HH), laid the basis for the use of magnification as a probe of cosmology and large scale structure.

In contrast to cosmic shear analysis, which has seen a recent concentrated effort by the lensing community to remove or understand measurement or statistical systematics, magnification bias as a probe of cosmology is relatively less mature. The reasons for this are simple, for a given sample of galaxies the signal to noise for magnification bias is expected to be smaller, as the shot noise in the shear case is reduced by factor of the intrinsic ellipticity dispersion for each ellipticity component (see Section). However it should be noted that we expect to be able to use a greater number of galaxies in a magnification analysis (provided accurate photometry is taken for these galaxies) than for cosmic shear, as the measurement itself is easier and does not require accurate shape measurement, and this should go some way to offsetting the discrepancy in signal to noise between shear and magnification. Magnification bias is mainly limited by errors in photometry. In particular, the amplitude of the number density contrast correlation from magnification is smaller than that induced by the intrinsic clustering of galaxies due to their dark matter environment. Previous analyses have attempted to remove most of this contamination by choosing carefully selected foreground and background populations which are spatially disjoint (such as HH, van Wearbeke or Scranton which chooses to use quasars as background as galaxy and quasar populations are generally well segregated in redshift), or in down weighting close pairs using the nulling technique (ref BJ and AH). Errors in the determination of the photometric redshift of a galaxy sample can then cause the intrinsic clustering of spatially close populations to be mis-interpreted as a magnification signal, giving spurious results. Further, dust extinction and fluctuation of the magnitude zero points over the survey area can produce fluctuations in number density that mimic the magnification signal, and remain relatively unexplored.

In this paper we consider the use of induced correlations in number density between tomographically binned samples of galaxies, including contributions from all binned galaxy distributions, as a probe of cosmology using a Fisher matrix analysis, which particular emphasis on what gains are made when combining a shear and magnification analysis. The theoretical predictions for the number density power spectra are set out in Section []. Information on the spectroscopic redshift distributions and number counts are taken from CFHT catalogues, described in Section [], and in Section [] we consider the optimal choice of magnitude cut, redshift binning and population selection for maximising the magnification signal and constraints. Concluding remarks and final discussion are presented in Section [].

2 TWO-POINT CORRELATIONS FROM MAGNIFICATION BIAS

2.1 Number Density Statistics

Deflection of light by intervening matter causes the observed number density of source bodies to be changed in two ways:

(i) The solid angle behind the lens is stretched by a factor of μ (where μ is the local magnification factor), thus the observed position of sources is changed leading to a dilution of sources behind a foreground over-density

(ii) The observed size of the source is changed, leading to an increase in the observed flux of the source as an application of Louiville's Theorem. The observed number density of sources may then change in a flux limited survey, as sources are (de-)amplified across this flux limit. This is equivalent to an effective change in the flux limit of the survey $S \rightarrow S/\mu$.

These two effects then modify the observed number counts of sources as

$$n(>S,\theta) = \frac{n_0(>S/\mu(\theta),\theta)}{\mu(\theta)}. \quad (1)$$

Assuming that the unlensed number counts follow a power law $n_0(>S) \propto S^{\alpha}$, equation (1) becomes:

$$n(>S) = \mu^{\alpha-1} n_0(>S) = [1+2(\alpha-1)\kappa(\theta)] n_0(>S) \quad (2)$$

where the weak lensing approximation $\mu \sim 1+2\kappa$ has been used. From equation (2) it is clear that when $\alpha = 1$ the overall magnification effect does not cause a change in the observed number density of sources, as the dilution of sources is perfectly balanced by the amplification of sources. Alternatively, when $\alpha \neq 1$ there will be an overall increase/reduction in the observed number of sources. It can be shown that

$$\alpha(m) = 2.5 \frac{d\, log\, n(>m)}{dm} \quad (3)$$

where we have changed to magnitudes instead of fluxes. Defining the number density contrast as $\delta n = (n-n_0)/n_0$, equation (2) states the fluctuation in observed number density due to magnification follows

$$\delta n_M(\theta) = 2(\alpha-1)\kappa(\theta) \quad (4)$$

and the observed number density contrast is then

$$\delta n^{(i)}(\theta) = \delta n_M^{(i)}(\theta) + \delta n_I^{(i)}(\theta) + \delta n_{rn}^{(i)}(\theta) \quad (5)$$

with δn_M the change in number density due to magnification, as given in equation (4), δn_I the contribution from the intrinsic clustering of the sources according to their dark matter environment, and δn_{rn} a random stochastic element. As surveys measure projected quantities across the sky, we consider projected number density contrast, defined for each term later, with redshift information from a tomographic analysis using photometric redshifts. Superscript in parenthesis denote a tomographic photo-z bin i.

As the convergence (and consequently number overdensity) vanish when averaged over large scales, the observed number density satisfies $\langle n \rangle = \langle n_0 \rangle$, and we consider two point correlations of these quantities. In particular, we consider the two point correlation of the Fourier coefficients of the convergence and number density contrast, related to the Power Spectrum P as:

$$\langle x^{(i)}(\ell) x^{(j)}(\ell') \rangle = (2\pi)^2 \delta_D(\ell-\ell') P_{xx}^{(ij)}(\ell) \quad (6)$$

for variable x. $\delta_D(\ell-\ell')$ is the two dimensional Dirac delta function, which illustrates the non-mixing of angular wavenumber (ℓ) modes due to isotropy and homogeneity.

Thus, from equation (5) we see that the observables in which we are interested follow:

$$P^{(ij)}_{\delta n\delta n}(\ell) = P^{(ij)}_{MM}(\ell) + P^{(ij)}_{II}(\ell) + P^{(ij)}_{MI}(\ell) + P^{(ij)}_{IM}(\ell) + \delta^{ij}_K S^{(ij)}_{\delta n} \quad (7)$$

$$P^{(ij)}_{\kappa_s\kappa_s}(\ell) = P^{(ij)}_{\kappa\kappa}(\ell) + \delta^{ij}_K S^{(ij)}_{\kappa_s} \quad (8)$$

$$P^{(ij)}_{\kappa_s\delta n}(\ell) = P^{(ij)}_{\kappa I}(\ell) + P^{(ij)}_{\kappa M}(\ell) \quad (9)$$

where δ^{ij}_K is the Kronecker delta function. For notational convenience I have suppressed the subscripts such that $\delta n_I \to I$ and $\delta n_M \to M$, and used the fact the stochastic term for the number density contrast and shear are uncorrelated with the other quantities and only contribute to the shot noise (S) in the autocorrelation term. When considering the shear-only signal, we assume that all the shape information is contained in the convergence field κ_s, defined as in equation (10). This should be a valid approximation as the shear and convergence power spectra are identical, $P_{\kappa\kappa} = P_{\gamma\gamma}$.

The projected convergence field is defined as

$$\kappa(\theta) = \int_0^{\chi_H} d\chi\, q^{(i)}(\chi)\delta_m(\theta,\chi) \quad (10)$$

with χ the comoving distance of the source, δ_m the dark matter over density, and the weight given as

$$q^{(i)}(\chi) = \frac{3H_0^2\Omega_m}{2c^2}\frac{f_K(\chi)}{a(\chi)}\int_\chi^{\chi_H} d\chi'\, p^{(i)}(\chi')\frac{f_K(\chi'-\chi)}{f_k(\chi')}. \quad (11)$$

$p^{(i)}(\chi)$ denotes the galaxy comoving distance probability distribution for tomographic redshift bin i, a the scale factor and $f_K(\chi)$ the angular diameter distance.

Similarly, the projected number density contrast due to intrinsic clustering is given by

$$\delta n_I(\theta) = \int_0^{\chi_H} d\chi'\, p^{(i)}(\chi)\delta n_I(\theta,\chi) \quad (12)$$

where the galaxy comoving distance probability distribution $p^{(i)}(\chi)$ is the same as that defined in (11). In using the same galaxy distribution in modelling the number density contrast as the shape convergence κ_s, we assume that the sample of galaxies used is restricted to those in which shape information is available, or that the galaxy distribution of the sample of galaxies used in shape measurement is representative of the galaxy distribution of the sample which may be used for magnification analysis. As shape measurement on a galaxy requires a higher signal to noise than required for magnification, we expect that a magnification analysis could use a larger sample of galaxies for surveys which take photometry on galaxies even when shape information cannot be resolved. This may be taken partly into account in the Shot Noise contribution to the number density contrast power spectrum, as described in Section ***, however we assume this has a negligible effect on the galaxy distribution.

The fluctuation due to intrinsic clustering is related to the matter over density via a bias term that can be scale or distance dependant, $\delta n_I(\theta,\chi) = b(\theta,\chi)\delta_m(\theta,\chi)$ so that the intrinsic clustering contribution to the power spectrum follows

$$P_{II}(k,z) = b^2(k,z)P_{\delta_m\delta_m}(k,z) \quad (13)$$

$$P_{I\delta_m}(k,z) = b(k,z)r(k,z)P_{\delta_m\delta_m}(k,z) \quad (14)$$

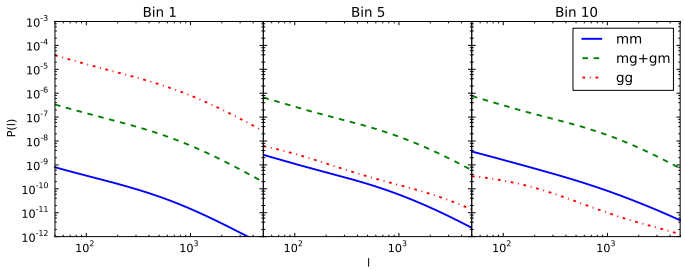

Figure 1. Contributions to the number density contrast power spectrum for a combination of background redshift bins, for binned galaxy distribution functions given in (ref). Foreground bin chosen to be redshift bin 1. It can be seen that for foreground and background that are spatially close in redshift, the overlap in redshift distribution due to redshift errors can easily cause the magnification terms (mg or mm) to be swamped by the intrinsic clustering term (gg). As we increase the separation in redshift between foreground and background, the amplitude of the gg term decreases whilst the cross (mg+gm) and mm term increase.

with $r(k,z)$ a stochastic bias which we take to be unity for the remainder of this paper, as stochastic bias can be shown to be close to unity on large scales (ref Gaztangaga).

All power spectra terms for projected quantities are related to the three dimensional dark matter power spectra using the Limber approximation in the flat sky limit. The contributions to the number density contrast power spectra in equation (7) are then

$$P^{(ij)}_{\kappa\kappa}(\ell) = \int_0^{\chi_H} d\chi\, \frac{q^{(i)}(\chi)q^{(j)}(\chi)}{f^2_K(\chi)} P^{(ij)}_{\delta_m\delta_m}\left(\frac{\ell}{f_K(\chi)},\chi\right) = P^{(ij)}_{\gamma\gamma}(\ell) \quad (15)$$

$$P^{(ij)}_{MM}(\ell) = 4(\alpha^{(i)}-1)(\alpha^{(j)}-1)P^{(ij)}_{\kappa\kappa}(\ell) \quad (16)$$

$$P^{(ij)}_{\kappa M}(\ell) = 2(\alpha^{(j)}-1)P^{(ij)}_{\kappa\kappa} \quad (17)$$

$$P^{(ij)}_{MI}(\ell) = 4(\alpha^{(i)}-1)\int_0^{\chi_H} d\chi\, \frac{q^{(i)}(\chi)p^{(j)}(\chi)}{f^2_K(\chi)} \times b\left(\frac{\ell}{f_K(\chi)},\chi\right) P^{(ij)}_{\delta_m\delta_m}\left(\frac{\ell}{f_K(\chi)},\chi\right) \quad (18)$$

$$P^{(ij)}_{IM}(\ell) = 4(\alpha^{(j)}-1)\int_0^{\chi_H} d\chi\, \frac{p^{(i)}(\chi)q^{(j)}(\chi)}{f^2_K(\chi)} \times b\left(\frac{\ell}{f_K(\chi)},\chi\right) P^{(ij)}_{\delta_m\delta_m}\left(\frac{\ell}{f_K(\chi)},\chi\right) \quad (19)$$

$$P^{(ij)}_{II}(\ell) = \int_0^{\chi_H} d\chi\, \frac{p^{(i)}(\chi)p^{(j)}(\chi)}{f^2_K(\chi)} \times b^2\left(\frac{\ell}{f_K(\chi)},\chi\right) P^{(ij)}_{\delta_m\delta_m}\left(\frac{\ell}{f_K(\chi)},\chi\right) \quad (20)$$

$$P^{(ij)}_{\kappa I}(\ell) = \int_0^{\chi_H} d\chi\, \frac{q^{(i)}(\chi)p^{(j)}(\chi)}{f^2_K(\chi)} \times b\left(\frac{\ell}{f_K(\chi)},\chi\right) P^{(ij)}_{\delta_m\delta_m}\left(\frac{\ell}{f_K(\chi)},\chi\right). \quad (21)$$

2.2 Shot Noise

The final contribution to the observed number density contrast power spectrum comes from the Shot Noise term, P_{SN} in equation (7), which is non-zero only when considering the

autocorrelation, when $i = j$, and takes the form

$$S^{(ij)}_{\delta n} = \delta^{ij}_K \frac{1}{\bar{n}^{(i)}}. \quad (22)$$

When considering the shear-only signal, this is modified to

$$S^{(ij)}_{\kappa_s} = \delta^{ij}_K \frac{\sigma^2_\epsilon}{2\bar{n}^{(i)}} \quad (23)$$

where σ_ϵ is the intrinsic ellipticity dispersion per component, typically $\sigma_\epsilon \sim 0.4$.

2.3 Parameter Forecasts

To estimate parameter constraints we use a Fisher Matrix analysis, where the Fisher Matrix is given as defined in (ref Tegmark):

$$F_{\alpha\beta} = \sum_r \frac{\ell_r d\ell_r \Delta\Omega}{4\pi} Tr[C^{-1}(\ell_r)C_{,\alpha}(\ell_r)C^{-1}(\ell_r)C_{,\beta}(\ell_r)] \quad (24)$$

where $C(\ell)$ is the covariance matrix for data vector $D(\ell)$ at angular wavenumber ℓ, with mean of zero, and where we have used the non-mixing of angular wavenumber modes in equation (6) to simplify the expression. $\Delta\Omega$ denotes the sky coverage area of the survey. Subscripts α and β run over the set of parameters we are considering, $\{\Omega_M, \Omega_{\rm Baryon}, \Omega_\lambda, w_0, {\rm H}_0, n_{\rm spec}, \sigma_8\}$ taken around WMAP7 fiducial values $\{0.3, 0.0456, 0.7, -1.0, 70, 1.0, 0.8\}$. We do not restrict ourselves to flat models, and the curvature is set by $\Omega_k = 1 - (\Omega_M + \Omega_\lambda)$.

We consider two types of data vector:

(i) For the shear only case, the data vector takes the form $D(\ell) = (\kappa^{(1)}_s(\ell), \ldots, \kappa^{(N_z)}_s(\ell))$, so that $C^{ij}(\ell) = P^{(ij)}_{\kappa_s\kappa_s}(\ell)$. Similarly, when considering clustering only, the data vector takes the form $D(\ell) = (\delta n^{(1)}(\ell), \ldots, \delta n^{(N_z)}_s(\ell))$, so that $C^{ij}(\ell) = P^{(ij)}_{\delta n\delta n}(\ell)$.

(ii) For the combination of a shear analysis with information from magnification, the data vector takes the form $D(\ell) = (\kappa^{(1)}_s(\ell), \ldots, \kappa^{(N_z)}, \delta n^{(1)}(\ell), \ldots, \delta n^{(N_z)}(\ell))$ so that the covariance matrix takes block form

$$C(\ell) = \left(\begin{array}{c|c} P_{\kappa_s\kappa_s}(\ell) & P_{\kappa_s\delta n}(\ell) \\ \hline P_{\delta n\kappa_s}(\ell) & P_{\delta n\delta n}(\ell) \end{array} \right) \quad (25)$$

with Power Spectra as defined in equation (7).

Throughout this paper we utilise a Figure of Merit (FoM) as a measure of the constraining power of either analysis considered above, defined as

$${\rm FoM_p} = \sqrt{\frac{1}{\det[F^{-1}]_p}} \quad (26)$$

where p denotes the subset of parameter space we are interested in. In this paper we consider two types of FoM:

(i) (${\rm FoM}_{DETF}$) A Dark Energy Task Force-like figure of merit, taking $p = \{\Omega_\lambda, w\}$

(ii) (${\rm FoM}_{Bias}$) taking $p = \{\Omega_M, \sigma_8\}$, chosen to be most sensitive to changes in the galaxy bias parameter.

3 MODELLING

3.1 Survey Modelling

3.2 Galaxy Bias

In section () we discussed briefly our parameterisation of the intrinsic clustering correlations using a galaxy bias parameter which can be both scale and redshift dependant, $b(k, z)$. As the galaxy bias in the non-linear regime is the least well know contribution to the power spectra in equation (), we discard any information from the non-linear regime that may inadvertently induce a strong signal from the intrinsic clustering term alone. To do this we utilise a similar technique to that in (ref BJ), and remove information at the Fisher matrix level by discarding any bias-dependant information above a certain ℓ-cut (ℓ_{max}), where

$$\ell_{max}(z^{(i)}) = f_K(\chi|_{z^{(i)}})k_{max}. \quad (27)$$

We choose the median redshift as the characteristic redshift for bin (i), $z^{(i)}$. k_{max}, the maximum wavenumber, is fit following a method similar to that presented in (ref Rassat et al) as $k_{max} = 1.4\pi/R$, where R is the radius beyond which

$$\sigma^2(R, z) = \int d\ \ln(k)\Delta^2(k, z)W^2(kR) < \sigma^2_R \quad (28)$$

and where $W(y) = 1/y[\sin(y) - y\cos(y)]$. Figure (ref Fig.) shows how k_{max} varies with redshift for different choices of σ_R, with smaller choices of σ_R giving more conservative cuts in wavenumber. Hereafter we chose to take ℓ-cuts by fitting k_{max} such that the matter density variance with a sphere of radius R is $\sigma(R, z) < 0.5$.

By allowing the cuts in angular wavenumber to be redshift dependant we try to ensure that we only cut out non-linear scales in each redshift bin, so we obtain an ℓ_{max} for each redshift bin considered. As the shear power spectra is not dominated by terms which include the galaxy bias, we do not impose these ℓ-cuts on the shear power spectrum. For the number density contrast power spectra $P^{(ij)}_{\delta n\delta n}$, we take the ℓ-cut corresponding to the lowest redshift bin, and for the shear-number density contrast power spectra $P^{(ij)}_{\kappa_s\delta n}$ we impose ℓ-cuts for the redshift bin from which number density information is obtained (in this example $\ell^{(j)}_{max}$).

To model the redshift dependance of galaxy bias, we assign a nuisance parameter to each redshift bin which can then be marginalised over. Each of this set of nuisance parameters are allowed to vary independently and without limit. We then use a set of N_z nuisance parameters for the galaxy bias, where N_z is the number of redshift bins being considered, each of which are assumed linear and taken at fiducial value $b^{(i)}_{fid} = 1.0$. By marginalising over these parameters we consider the case where the galaxy bias is completely unknown. Alternatively, we consider the case with the galaxy bias fixed at it's fiducial value, corresponding to fully known galaxy bias.

In a third scenario we add a prior on the galaxy bias, where the covariance matrix of the galaxy bias parameters

is constructed to take the form:

$$C_{\rm Bias} = \sigma_r^2 \begin{pmatrix} 1 & r & r^2 & r^3 & \cdots & r^{N_z-1} \\ r & 1 & r & r^2 & \cdots & r^{N_z-2} \\ \vdots & & \ddots & & & \vdots \\ r^{N_z-1} & r^{N_z-2} & r^{N_z-3} & r^{N_z-4} & \cdots & 1 \end{pmatrix}. \tag{29}$$

where σ_r is allowed to vary as a function of r as

$$\sigma_r = \sigma_0 \left[\frac{N_z - (N_z-2)r}{N_z(1+r)} \right]^{\frac{1}{2}} \tag{30}$$

to ensure 1-σ errors on each bias parameter are independent of r (see Appendix A). Here r gives the strength of the correlation between adjacent bins, and σ_0 the uncertainty of each bias parameter. This prior is then added to the Fisher Matrix constructed as in section () as

$$F_{\alpha\beta} \to F_{\alpha\beta} + (C^{-1}_{\alpha\beta})_{\rm Bias}. \tag{31}$$

where in this case α and β run only over the bias parameters, $\alpha, \beta = \{b^{(1)}, \cdots, b^{(N_z)}\}$, and all elements corresponding to all other parameters are left unchanged.

By correlating each bias parameter to its neighbours as the correlation strength to the power of the difference in redshift bins we define a correlation length, equivalent to the redshift over which the bias becomes uncorrelated. By increasing the strength of the correlation, we reduce the freedom each bias parameter has with respect to it's neighbour, thus reducing the variance of bias nuisance parameters across redshift bins. This reduces the ability of individual bias parameters to vary independently of each other, thus making the function of bias versus redshift smoother and more realistic. We therefore expect that as we increase the correlation strength ($r \to 1$), we should improve cosmological constraints from magnification as we retain more information from the clustering of sources, and increase the value of a FoM using cosmological parameters. As we expect galaxy bias to be a smooth function in redshift, we do not expect galaxy bias parameters between adjacent redshift bins to be negatively correlated, and we consider only $0 \leqslant r \leqslant 1$.

The parameter σ_0 gives the marginal error on each bias nuisance parameter when fully uncorrelated ($r = 0$). As such, σ_0 gives the scatter on the value of the bias in each redshift bin, and is assumed to the the same across all redshift bins considered. Therefore, σ_0 sets the level of uncertainty on each galaxy bias parameter, and we expect that we increase the uncertainty in galaxy bias, the constraining power from magnification is reduced as less information from the clustering signal is accessible, and conversely as $\sigma_0 \to 0$ and we recover fully known galaxy bias.

3.3 Galaxy Redshift Distributions

We model the galaxies distributions in spectroscopic redshift as

$$p^{(i)}(z_s) = \int_{z_l^{(i)}}^{z_h^{(i)}} d\, z_{ph} p(z_s|z_{ph}) p(z_{ph}) \tag{32}$$

where $p(z_s|z_{ph})$ is described by a Gaussian with width $\sigma_z = 0.05(1+z_{ph})$ which describes the photometric redshift errors. $p(z_{ph})$ gives the galaxy redshift distribution as measured for photometric redshift, and is modelled as [ref Smail et al)

$$p(z_{ph}) = \left(\frac{z_{ph}}{z_0} \right)^{\alpha'} \exp^{-\left(\frac{z_{ph}}{z_0}\right)^{\beta}} \tag{33}$$

with characteristic redshift z_0 related to the median redshift of the survey by $z_0 = z_{med}/1.412$. Figure (ref Fig.) shows the resultant galaxy distribution for !!N!! redshift bins between $z_{ph} = [0, 2]$, with the resultant number density contrast power spectra given for three choices of bin combination in figure (ref Fig.). Noticeably, for closely separated redshift bins, the intrinsic clustering term in non-vanishing, and the intrinsic clustering-magnification cross term is dominant to the pure magnification power spectra, due to the presence of photometric redshift errors with cause some galaxies to be incorrectly assigned to a given redshift bin, and causes overlap between bins. As we take redshift bins that are more widely separated, the power from intrinsic clustering decreases, so we see that for the most widely separated bins the total power is dominated by terms that include the magnification. As the cross power is always dominant to the pure magnification power, frequently studies will ignore the pure magnification contribution to the overall clustering power, and instead just quote the cross contribution, usually in the situation where correlations are considered between distant foreground and backgrounds, so the intrinsic clustering contribution is subdominant and may also be ignored. In this analysis, we consider all contributions to the power, as given in equation (eqn ref).

Measurements required for a magnification bias analysis are expected to be easier than those required for a cosmic shear analysis, as we do not require the accurate measurement of galaxy ellipticity which can be affected by the PSF, pixel noise and other complicating systematics. Rather, the use of magnification bias requires only the identification of galaxies, and accurate photometry. Consequently, we expect the sample size of galaxies used in a magnification bias analysis to be larger than that used in cosmic shear for surveys where photometry is taken for all galaxies, not only for those for whom shape can be measured to the required level for a cosmic shear analysis, resulting in a difference to the galaxy distributions used for either analysis, and a change in the number density of sources which affects the statistical noise through the shot noise part of the power spectrum, as defined in Section [ref].

We account for this change in sample size by considering a change in the signal to noise cut, above which galaxies are included in the sample, and which corresponds to a change in the maximum magnitude to which galaxies are included in the sample. Using CFHT catalogues covering 154 deg^2 of the sky, we determine the following relations between the median redshift of the sample and the number density of sources in the sample

$$\Delta z_{med} = 0.07 \Delta M \tag{34}$$

with $\Delta M = M^{\delta n} - M^{\kappa_s}$, M denotes the magnitude cut, and $\Delta z_{med} = z_{med}^{\delta n} - z_{med}^{\kappa_s}$, and

$$n_g = n_g^{\kappa_s} \left(\frac{z_{med}^{\delta n}}{z_{med}^{\kappa_s}} \right)^5. \tag{35}$$

A difference in signal to noise cuts of 2.5 corresponds to a magnitude limit difference of ~ 1.

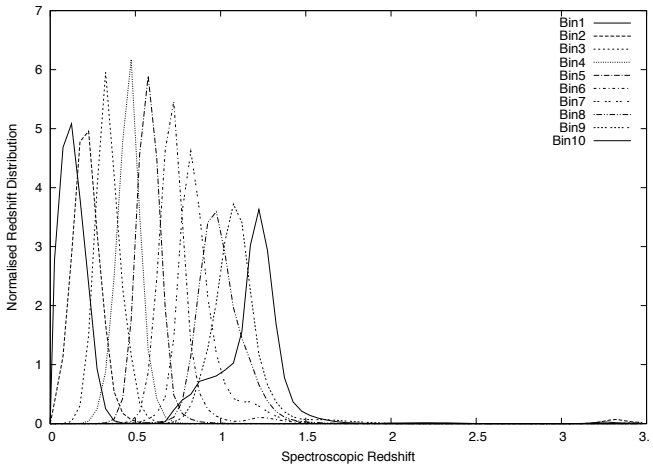

Figure 2. Galaxy Redshift distributions from CFHT data, including catastrophic redshifts for given galaxy sample selection and for all redshift bins. Should not be too busy by nature, as plots should only overlap in a small region.

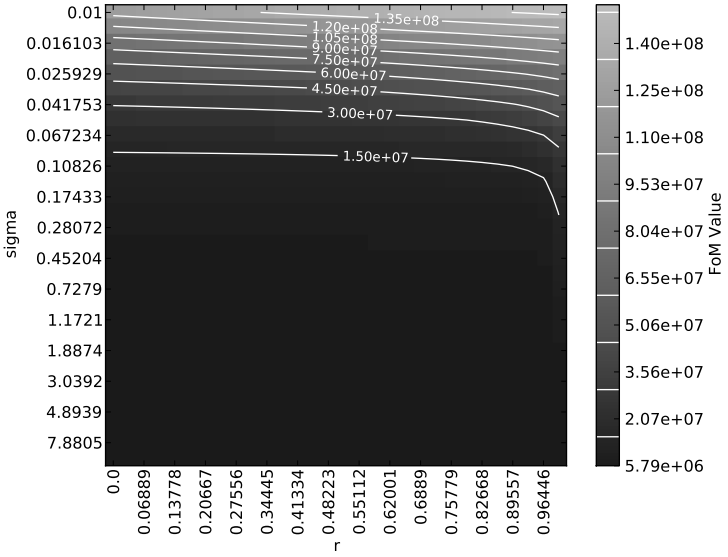

Figure 6. Contour plot showing constant-FoM contours as a function of σ and r (Uncertainty and correlation in Bias Prior). Point details choice of σ and r from external probe.

3.5 Optimisation

4 RESULTS

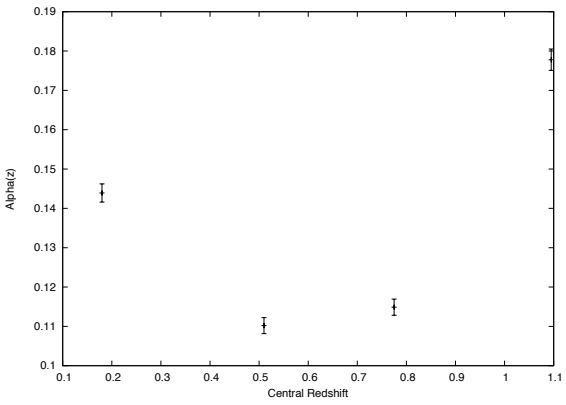

Figure 4. Alpha as a function of redshift for the redshift bins chosen, for magnitude limits motivated by previous signal to noise plot.

3.4 The Slope of the Number Counts of galaxies

In choosing the values for the slope of the number counts (α) which sets the strength of the magnification effect, we first calculate values for α using CFHTLenS catalogues.

CFHTLenS is based on the Wide part of the Canada-France-Hawaii-Telescope-Legacy-Survey, and covers 154 deg^2, (125 deg^2 after masking) of the sky in the five $u^*g'r'i'z'$ filters. We consider...

Figure (ref Fig.) shows $\alpha - 1$ as a function of magnitude limit for three redshift bins.

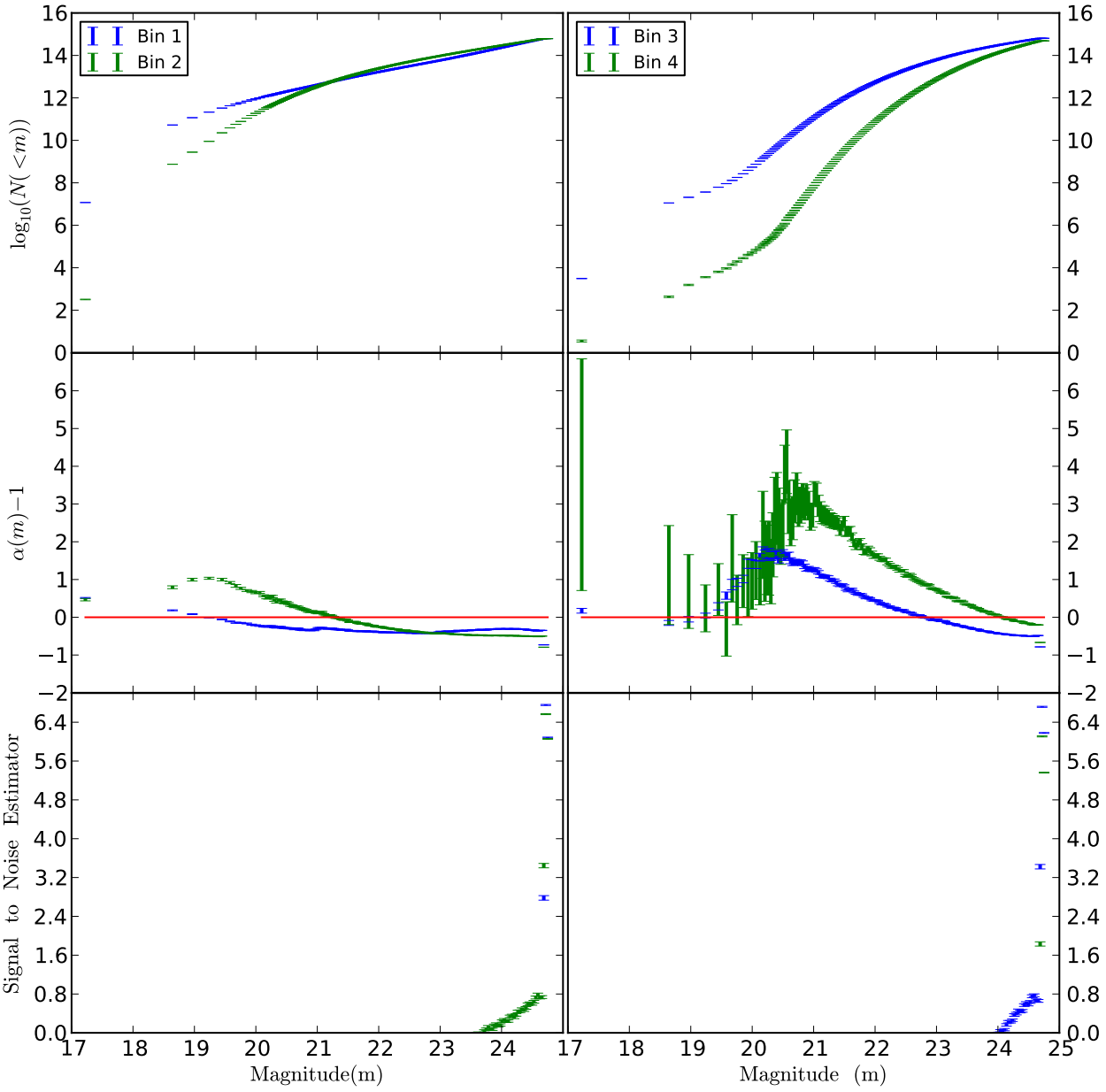

Figure 3. The log of the cumulative number counts, Slope of Cumulative Number counts (defined in) and the Signal to Noise estimator (defined..) as a function of limiting magnitude, for redshift bins as described in (). All quantities are derived for CFHTLS catalogues, over 160 patches, as discussed in (Section Reference). For illustrative purposes, the plot of $\alpha-1$ shows $\alpha-1=0$, where the magnification signal is expected to be identically zero. As the we consider fainter limiting magnitudes, the signal to noise estimator increases as the increase in cumulative number density dominates. This suggests that we should always consider magnitude cuts that are as faint as possible, provided this avoids an area where $\alpha-1=0$.

5 CONCLUSIONS

ACKNOWLEDGMENTS

REFERENCES

Bibliography here

APPENDIX A: THE GALAXY BIAS PRIOR - NORMALISING THE LIKELIHOOD

We define the covariance matrix for the prior on N_z linear galaxy bias parameters as in equation (ref). The covariance matrix then takes the form $C=\sigma_r^2 R$, where R is the matrix of correlation parameters in Toeplitz form. The full likelihood for the bias parameters then follows:

$$\frac{p(\bar{b})}{p(\bar{0})}=e^{-\frac{1}{2}\chi^2} \tag{A1}$$

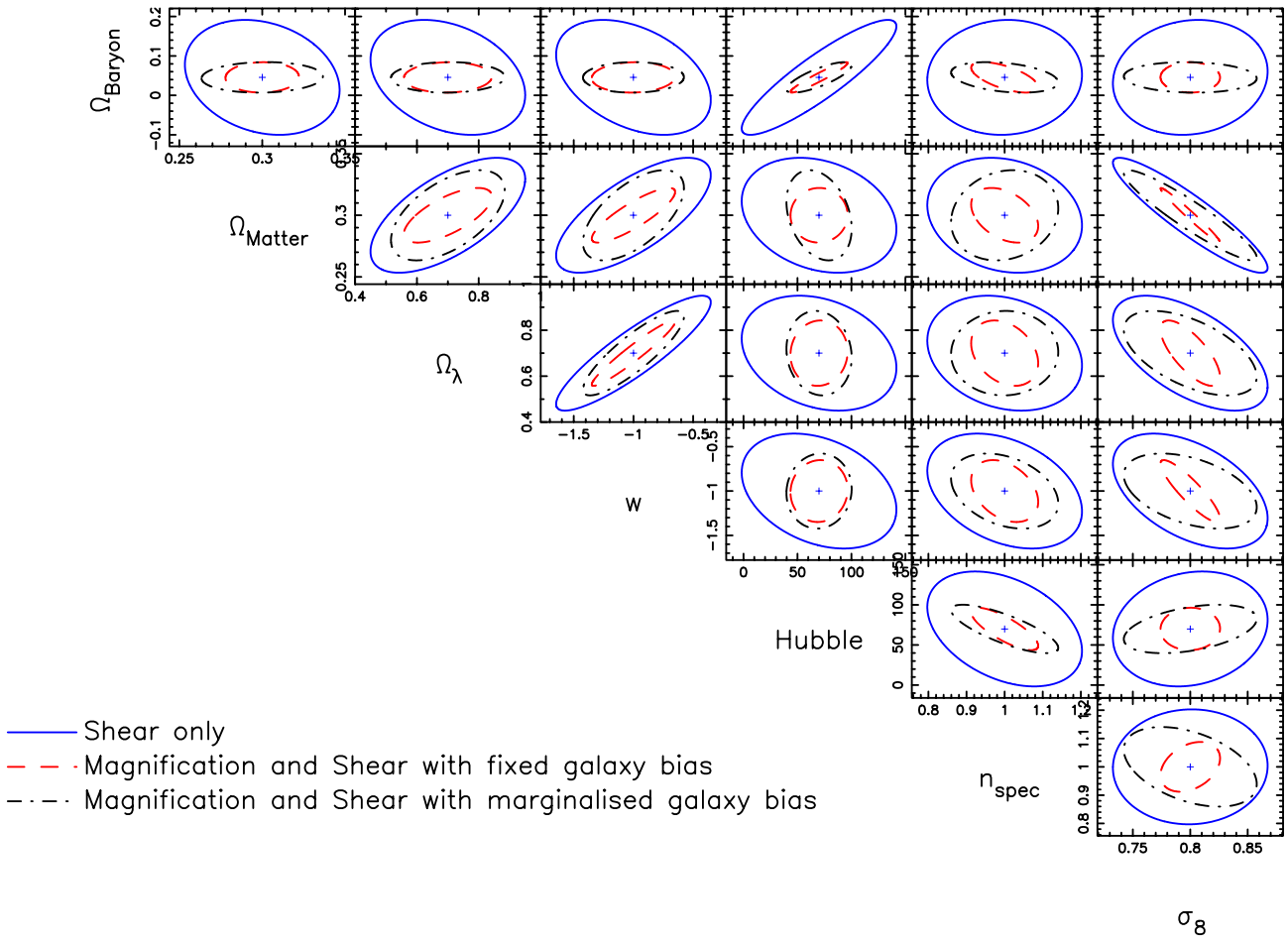

Figure 5. Contour plot for fully optimised magnifcation signal showing shear, and combined probe taking a known and fully unknown galaxy bias.

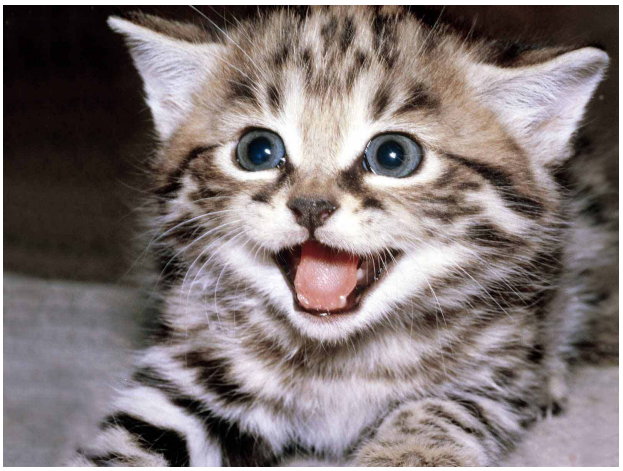

Figure 9. FoM vs number of redshift bins - gain in information by increasing redshift information - Optimisation.

with $\chi^2 = \bar{b}C^{-1}\bar{b}^T$ and satisfies

$$\chi^2 = \sum_{ij}^{n} b^2 (C^{-1})_{ij} \tag{A2}$$

along the line $b_1 = b_2 = \cdots = b_{N_z} = b$. It follows that

$$\chi^2 = \frac{b^2}{\sigma^2}\sum_{ij}^{n}(R^{-1})_{ij} = \frac{b^2}{\sigma^2}\sum_{ij}^{N_z}\left(\frac{Adj(R)}{det(R)}\right)_{ij} \tag{A3}$$

$$= \frac{b^2}{\sigma^2 det(R)}\sum_{ij}^{N_z}(Co(R)^T)_{ij} = \frac{b^2}{\sigma^2 det(R)}\sum_{ij}^{N_z}(Co(R))_{ij} \tag{A4}$$

where $Adj(R)$ denotes the adjoint matrix of R, $Co(R)$ the matrix of cofactors, defined as $Co_{ij} = (-1)^{i+j}M_{ij}$, M the minor matrix of determinants, and we have used the symmetry of R to note that $Co(R)^T = Co(R)$.

By symmetry, $Co(R)$ satisfies

$$Co(R) = \begin{pmatrix} x_1 & x_2 & 0 & 0 & \cdots & 0 \\ x_2 & x_3 & x_2 & 0 & \cdots & 0 \\ 0 & x_2 & x_3 & x_2 & \cdots & 0 \\ \vdots & & \ddots & & & \vdots \\ 0 & \cdots & 0 & 0 & x_2 & x_1 \end{pmatrix} \tag{A5}$$

so that

$$\sum_{ij}^{n} Co(R)_{ij} = 2x_1 + 2(N_z - 1)x_2 + (N_z - 2)x_3. \tag{A6}$$

and $det(R) = (1 - r^2)^{N_z - 1}$. x_1 is the determinant of the

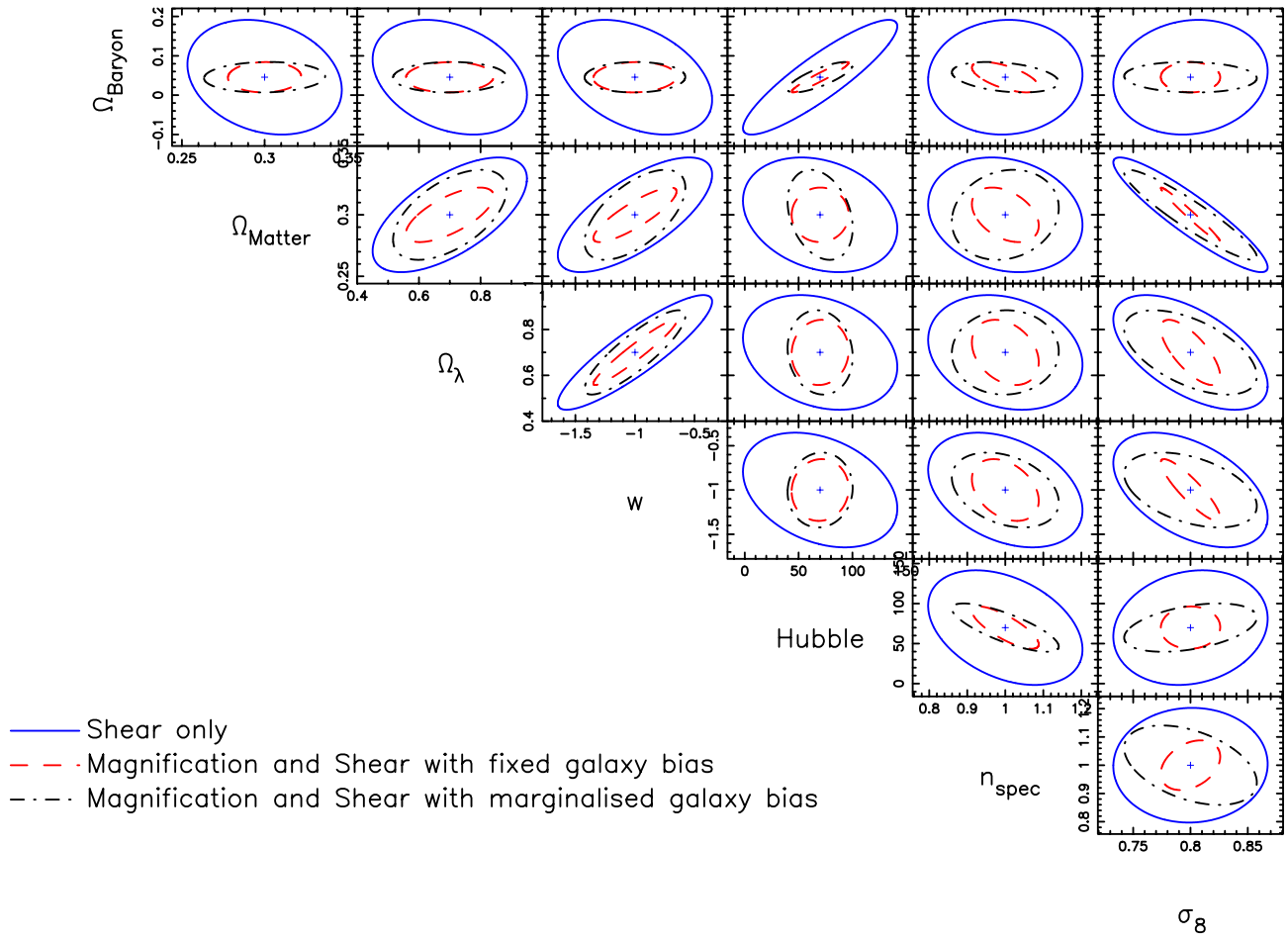

Figure 7. Contour plot showing fully optimised combined probe versus shear-only for choice of bias prior parameters.

$N_z - 1$ case of the matrix R, which I denote as $det(R^{(N_z-1)})$. The remaining factors can be calculated by noting that

$$\sum_j^{N_z} R_{ij} Co(R)_{ij} = det(R) \tag{A7}$$

so that

$$x_2 = \frac{1}{r}[det(R^{(N_z)}) - det(R^{(N_z-1)})] \tag{A8}$$

$$x_3 = 2det(R^{(N_z-1)}) - det(R^{(N_z)}). \tag{A9}$$

Using equations (A6) and (A3), we find that

$$\chi^2 = \frac{b^2}{\sigma_r^2}\left[\frac{N_z - (N_z-2)r}{1+r}\right]. \tag{A10}$$

It is clear then that if we keep σ_r constant with r, χ^2 at a given point along the $b_1 = b_2 = \cdots = b_{N_z} = b$ line will vary with r causing a change in the volume of galaxy bias parameter space probed by $1-\sigma$ contours to also vary with the correlation strength. We therefore normalise χ^2 along $b_i = b$ by choosing σ_r such that $\chi^2_r = \chi^2_{r=0}$ for all values of r. Noting that $b = \sigma_0/\sqrt{N_z}$ and requiring that $\sigma_r(r=0) = \sigma_0$, we find that

$$\sigma_r = \sigma_0\left[\frac{N_z - (N_z-2)r}{N_z(1+r)}\right]^{\frac{1}{2}} \tag{A11}$$

as stated in equation (30).

This paper has been typeset from a TEX/ LATEX file prepared by the author.

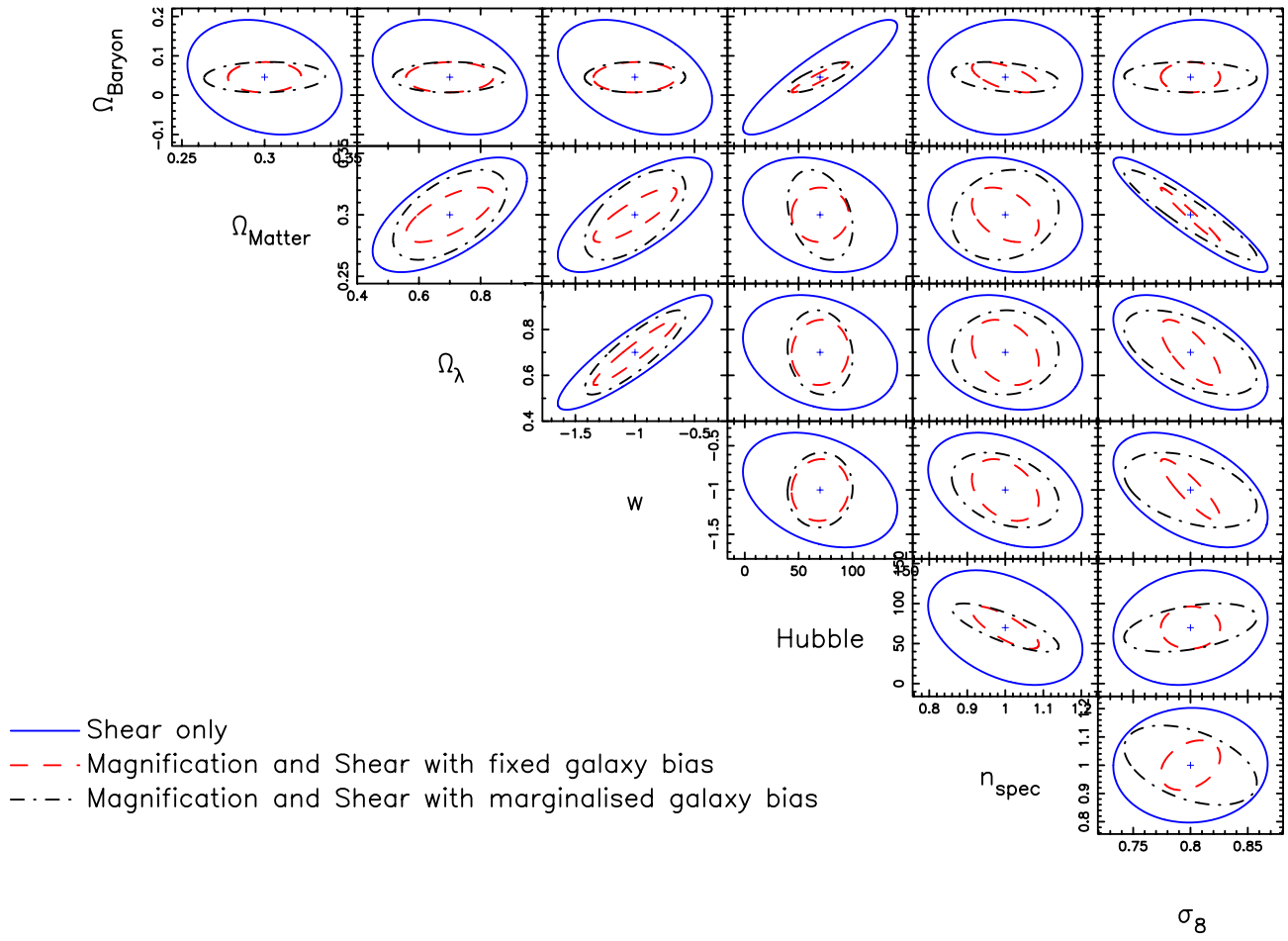

Figure 8. Contour plot showing fully optimised combined probe versus shear-only for choice of bias prior parameters with Planck Prior. - using old contour plot as placeholder